RSC Advances

PAPER

Preparation of TiO$_2$/Ti$_3$C$_2$T$_x$ hybrid nanocomposites and their tribological properties as base oil lubricant additives

Maoquan Xue,*[a] Zhiping Wang,[a] Feng Yuan,[a] Xianghua Zhang,[b] Wei Wei,*[c] Hua Tang[d] and Changsheng Li[d]

TiO$_2$/Ti$_3$C$_2$T$_x$ hybrid nanocomposites were successfully prepared by a facile liquid phase synthesis technology. The phase structure and morphology of as prepared samples were analyzed by means of X-ray diffraction and scanning electron microscopy. The results revealed that uniform TiO$_2$ particles were distributed within the surface and edge of Ti$_3$C$_2$T$_x$ nanosheets. Subsequently, the tribological properties of the TiO$_2$/Ti$_3$C$_2$T$_x$ hybrid nanocomposite as lubricant additive in base oil were evaluated with a UMT-2 ball-on-disc tribotester, and the morphologies of worn steel surfaces were investigated using a scanning electron microscope and non-contact optical profile testing instrument. The results of the friction tests showed that base oil with 1 wt% TiO$_2$/Ti$_3$C$_2$T$_x$ hybrid nanocomposite under optimal load had excellent friction reduction. The morphology of the worn surface analyzed by SEM and non-contact optical profile testing confirmed that the hybrid nanocomposites mended the scratched surface and formed a uniform tribofilm, thereby helping to improve the tribological properties of the base oil. Furthermore, this work shows the promising applications of TiO$_2$/Ti$_3$C$_2$T$_x$ hybrid nanocomposites in the field of tribology.

1. Introduction

In recent decades, ternary nanolaminated hexagonal ceramics M$_{n+1}$AX$_n$, where M is an early transition metal, A is an A-group element (mostly IIIA and IVA), and X is C and/or N, $n = 1, 2, 3…$,[1–5] have attracted great attention owing to their interesting properties and prospective applications.[6,7] As an important representative member of M$_{n+1}$AX$_n$, Ti$_3$AlC$_2$ has excellent ceramic and metallic properties, such as low coefficient of friction, excellent thermal and electrical conductivity, easy machinability, high elastic modulus, chemical stability, good thermal stability and oxidation resistance,[8–13] and has drawn mounting attention from researchers.

The laminated structure of Ti$_3$AlC$_2$ is comprised by alternative stacking of hexagonal TiC layers and congested edge-sharing bidimensional Al atomic layers along the *c*-axis, in which the bonding between Ti and C is firmly covalent, but the metallic bonding between Ti and Al is comparatively weak and therefore more susceptible to chemical reaction.[14–16]

Lately, Naguib *et al.*[17,18] reported to fabricate two-dimensional Ti$_3$C$_2$(OH)$_2$ nanosheets by selectively etching the Al layers with hydrofluoric acid (HF), following a similar process, other MAX phases have also been successfully exfoliated into the two-dimensional transition metal nanocarbides and nanonitrides named Mxenes,[19–21] theoretical and experimental investigation revealed that their properties distinct from those of their 3D MAX counterparts.[22–29]

Over the past decades, TiO$_2$, as a typical member of inorganic transition metal dioxides, has aroused numerous studies due to its attractive functional properties and promising applications. Furthermore, various hybrid modifications including surface modification, coupling with porous materials, and carbon coating have been executed to TiO$_2$ nanostructures in order to improve the properties. At present, several attempts have been made in the syntheses and properties of TiO$_2$ hybrid nanostructures. Soraya Hosseini *et al.*[30] studied the mesoporous carbon and TiO$_2$ photoanodes synthesized by sol–gel spin coating onto a glassy substrate, and found that the enhanced humic acid removal of TiO$_2$/C/C/TiO$_2$ photoanodes was due to the highest photocurrent density generated. Hong Z *et al.*[31] fabricated the TiO$_2$@C–rGO hybrid nanostructures through *in situ* growth of oriented self-assembly of TiO$_2$ mesocrystals on GO route, the hybrid nanostructures display a high reversible capacity, superior rate capability, and long term cycling stability, which is largely attributed to the strong architecture of well-dispersed carbon-coated mesoporous TiO$_2$ mesocrystals anchored on conductive graphene network. Wongaree M *et al.*[32]

[a]*Changzhou Vocational Institute of Light Industry, Changzhou, Jiangsu Province, 213164, P. R. China. E-mail: xuemaoq@163.com*

[b]*School of Mechanical Engineering, Jiangsu University of Technology, Changzhou, Jiangsu Province, 213001, P. R. China*

[c]*School of Materials Science and Engineering, Changzhou University, Changzhou, Jiangsu Province, 213164, P. R. China. E-mail: benjamin.wwei@163.com*

[d]*School of Materials Science and Engineering, Jiangsu University, Zhenjiang, JiangsuProvince, 212013, P. R. China*

prepared CNT/TiO_2 nanofibers by spinning CNT/poly(vinyl pyrrolidone) (PVP) solution followed by the removal of PVP, the synergistic effects of the larger surface area and lower band gap energy of CNT/TiO_2 nanofibers were presented as robust adsorption ability and greater visible light adsorption. Qian L et al.[33] produced biomorphic charcoal/TiO_2 composites from moso bamboo templates, the C/TiO_2 composites were exhibited lower geometrical density, better thermostability, and favorable microwave absorptive properties. Naguib M[34] and Gao[35] et al. fabricated TiO_2/C nanohybrids by mild oxidation of Ti_3C_2, the obtained samples were exhibited extremely high cycling rates when tested as anodes and good photocatalytic activity. However, $TiO_2/Ti_3C_2T_x$ hybrid nanostructures and their application in the tribiological field have rarely been reported.

In this work we report a simple method to prepare $TiO_2/Ti_3C_2T_x$ via immersing $Ti_3C_2T_x$ powders in distilled water assisted hydrothermal reaction. Moreover, the tribological properties of $TiO_2/Ti_3C_2T_x$ composites as additives in the base oil were also investigated. This study will be useful for Mxene practical application in the future.

2. Experimental

2.1 Synthesis of $TiO_2/Ti_3C_2T_x$ composites

To fabricate the Ti_3AlC_2 powders, commercially powders of Ti (99.0 wt% purity, 40 μm), Al (99.97 wt% purity, 75 μm), and graphite (99.85 wt% purity, <30 μm), Sn (>99.0 wt% purity, 40–75 μm) were mixed with the stoichiometric ratios of 3Ti/1Al/1.8C/0.2Sn, the specific preparing procedure was detailed in our previous study.[3] Briefly, powders in the appropriate proportion were magnetic stirring in absolute alcohol at 70 °C. After being dried and sieved, the powders were cold-pressed at 30 Mpa and then heated at 1450 °C under Ar for 20 min in a tube furnace, then taken out after cooling down to room temperature. The obtained Ti_3AlC_2 was crushed and sieved through a 300 mesh sieve.

To exfoliate the Ti_3AlC_2 to $Ti_3C_2T_x$ (Mxenes), 5 g Ti_3AlC_2 powders was immersed in a 40 wt% aqueous hydrofluoric acid solution, and magnetically stirring for 100 h at room temperature. Afterwards the etched powder mixtures were filtered and washed with ethanol and distilled water several times, and dried to obtain $Ti_3C_2T_x$ powders.

$TiO_2/Ti_3C_2T_x$ hybrid nanostructures were synthesized using a hydrothermal process. The prepared $Ti_3C_2T_x$ was added to distilled water and stirring evenly, then the solution was transferred to a Teflon-lined autoclave and placed in an electric oven heated at 200 °C for different time. After the hydrothermal process, the as-prepared product was washed with distilled water and ethanol for several times and then dried at 60 °C for 12 h. Finally, black powders were obtained.

2.2 Characterisation of samples

The X-ray diffraction (XRD) experiments on the $TiO_2/Ti_3C_2T_x$ were performed on a Bruker D8 advance diffractometer under CuKa radiation. The 2θ range used in the measurement was from 7 to 70°, data analysis with Jade software. The morphologies and structures were investigated using a JSM-7001F

scanning electron microscope (SEM). All the measurements were carried out at room temperature.

2.3 Tribological properties of $TiO_2/Ti_3C_2T_x$ as lubrication additive

The as-prepared $TiO_2/Ti_3C_2T_x$ hybrid nanocomposites were scattered to the base oil by mass fraction of 0.6 wt%, 1 wt%, 3 wt% and 5 wt%. Solid powders were uniformly dispersed in the base oil with ultrasonic generator and formulated into turbid liquid samples. Tribological properties of the base oil and mixed oil samples containing different mass fractions of additives were studied with a universal ball on disc micro-tribotester (UMT-2, Center for Tribology Inc, USA). The friction and wear tests were conducted at a rotary speed of 150 rpm and ambient temperature of about 25 °C for 10 min. The load was in the range from 5 N to 50 N. The stainless steel ball with a diameter of 10 mm and a hardness of 62 HRC was made of 440C stainless steel and the counterpart is 45 steel disc of Φ 30 mm × 3 mm in size. The friction coefficients were recorded automatically and the grinding cracks were measured by a JSM-5600LV scanning electron microscope (SEM) and a BRUKER ContourGT non-contact 3D optical profile testing instrument.

3. Results and discussion

The XRD patterns of the initial 3Ti/1Al/1.8C/0.2Sn mixture after heated at 1450 °C for 20 min. (Fig. 1a) show that the synthesized
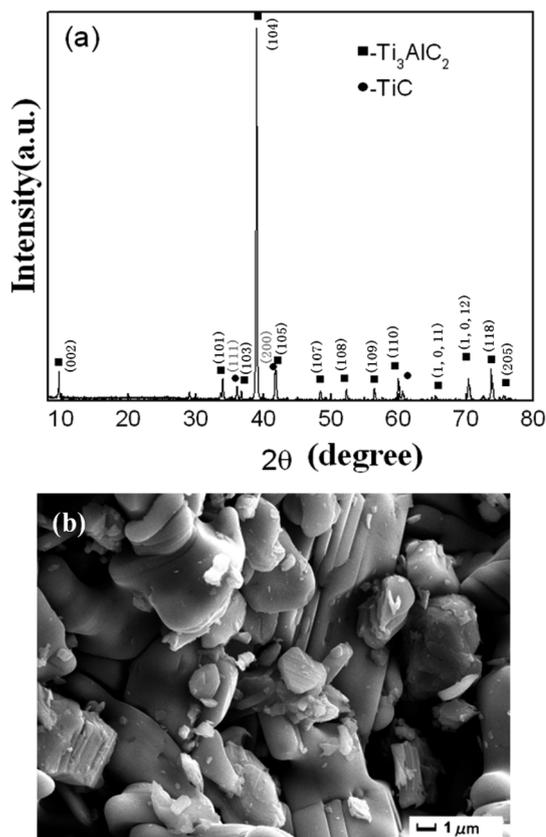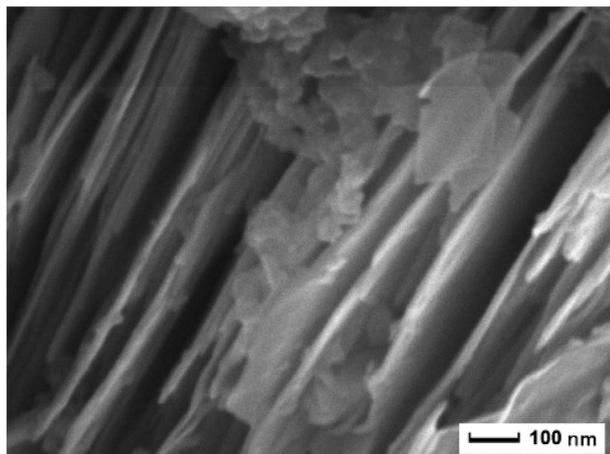

Fig. 1 XRD pattern and SEM morphology of Ti_3AlC_2.

Fig. 2 A typical SEM morphology of the synthesized multilayers $Ti_3C_2T_x$.

powders mainly contain Ti_3AlC_2 with small amounts of TiC as a secondary phase. The characteristic diffractions of Ti_3AlC_2 were detected around 9.5° and 39.0°, respectively, corresponding to the (002) and (104) planes, which are consistent with the previous literature[28] and the data in the standard card (JCPDS: 52-0875) for Ti_3AlC_2. According to the calculation from the XRD pattern, the purity of the sample is upto 96.7 wt%.

The size and morphology of Ti_3AlC_2 sample were identified by SEM. Fig. 1b shows the SEM images of the as-prepared Ti_3AlC_2 sample. Fig. 1b reveals that the sample consists of a lot of densely aligned laminated-like structure and smooth surface. Further observation shows that the particles have melting imprint, indicating the formation of liquid phase at high temperature,[3] the result indicating that high-yield and good morphology of Ti_3AlC_2 could be readily achieved through this approach.

Fig. 3I gives the XRD patterns of the exfoliated $Ti_3C_2T_x$ powders obtained by 40% HF treatment. After HF treatment, the labelled diffraction peaks in Fig. 3I can be indexed to those of the phase of $Ti_3C_2T_x$ and TiC,[17] the peaks indexed to Ti_3AlC_2 have clearly vanished. The XRD patterns of product verify the formation of $Ti_3C_2T_x$ phase.[28,36,37] The strong peaks were found around 9.0° and 18.2° corresponding to (002) and (004) of $Ti_3C_2T_x$, which shift to lower 2θ angles contrasting to the diffraction of Ti_3AlC_2, manifesting the expansion along c-axis. Owing to the weak metallic bonding between Ti and Al, the Al layer is exfoliated by selective etching off Ti_3AlC_2.[28] SEM images (Fig. 2) show that the obtained samples are uniform separated layers with an average thickness of about 10 nm.

Fig. 3 gives the X-ray diffractograms of $Ti_3C_2T_x$ before and after hydrothermal treatment in distilled water at 200 °C. The XRD patterns of the products of $Ti_3C_2T_x$ after treatment at 200 °C for 12 h can be indexed for both TiO_2 and $Ti_3C_2T_x$, in addition, it also can be clearly seen that the intensity of TiO_2 peaks increased as the reaction time increasing, while the fraction of not oxidized $Ti_3C_2T_x$ was greatly reduced. This reveals the kinetics of the oxidation process as a carbide consuming mechanism.[34]

Fig. 4 exhibits a typical SEM images for $Ti_3C_2T_x$ sample treated at 200 °C for 24 h. It can be seen from Fig. 4a that there are many uniform oxide particles distributing within the surface and edge of the thinner layers, while the original microstructure of $Ti_3C_2T_x$ is separately layered structure (Fig. 2). The magnified SEM image (Fig. 4b) further gives the details of hybrid nanocomposite. There are significant amounts of TiO_2 co-exist with $Ti_3C_2T_x$, the size of TiO_2 particles is about 100 nm.

In order to discuss the evolutions of the friction coefficients of $TiO_2/Ti_3C_2T_x$ hybrid nanocomposites, the concentration of the nanocomposites in the lubricant was studied. Several concentrations in the range from 0.6 wt% to 5 wt% were chosen. And the tests were carried out with 20 N, 150 rpm, 600 s and the
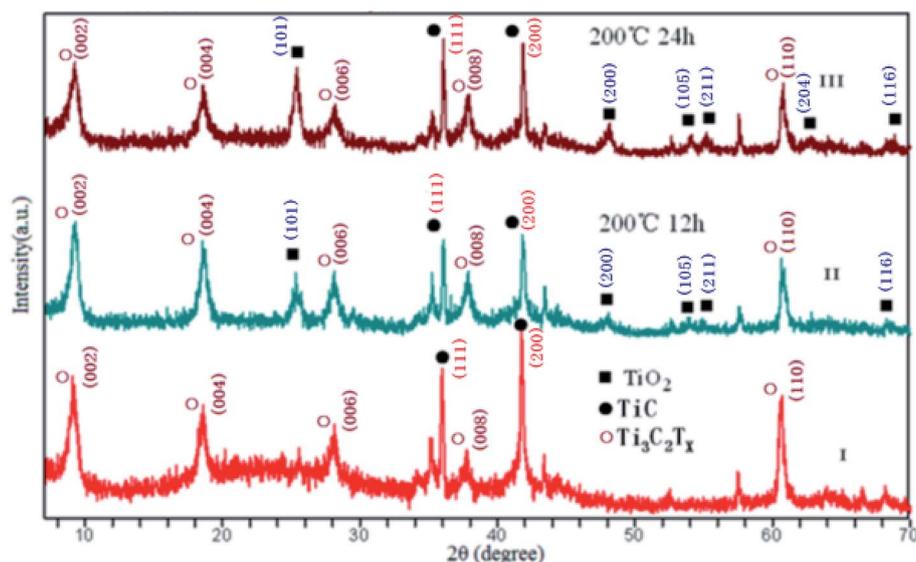

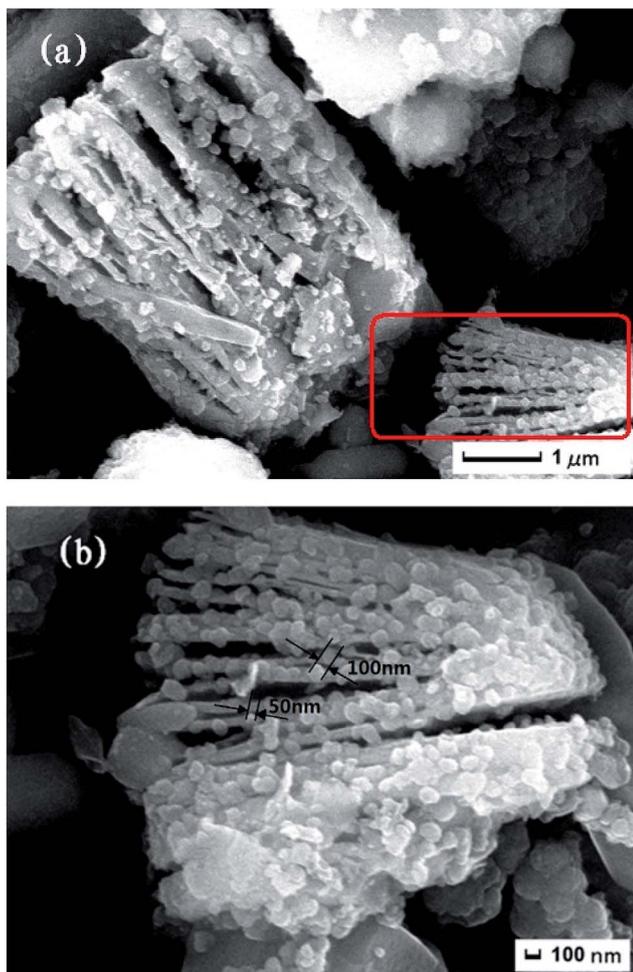Fig. 3 XRD patterns of $Ti_3C_2T_x$ before and after hydrothermal treatment at 200 °C for 12 h and 24 h.

Fig. 4 SEM images of $Ti_3C_2T_x$ after hydrothermal treatment in water at: (a) 200 °C for 24 h, and (b) zoom in on the region framed in (a).

Fig. 5 Friction coefficient as a function of sliding time lubricated with different concentrations $TiO_2/Ti_3C_2T_x$ hybrid nanocomposites in base oil (a) and base oil mixed with 1.0 wt% $TiO_2/Ti_3C_2T_x$ additive under different loads (b).

room temperature, respectively. The friction coefficients of the tests are offered in Fig. 5a. It can be seen that under base oil lubrication, the friction coefficient has a decreasing trend over 300 s, and then stabled with an average value of 0.103. The base oil with 0.6 wt% $TiO_2/Ti_3C_2T_x$ hybrid nanocomposites lubrication has the same trend with the base oil lubrication, maintained a friction coefficient of approximately 0.075 after 300 s sliding. The base oil with 1 wt% $TiO_2/Ti_3C_2T_x$ lubrication showed the lowest friction coefficient of 0.073 with a slight decreasing trend. This may be because, with the continuous sliding, more and more $TiO_2/Ti_3C_2T_x$ were adhered to the friction surfaces creating a tight layer between the two contact surfaces, leading to a reducing friction coefficient. However the friction coefficient of base oil with 3 wt% concentration became erratic and lifted along sliding time after 150 s sliding. When the base oil formulated with 5 wt% $TiO_2/Ti_3C_2T_x$, the friction coefficient rose observably over 0.16 and an increasing trend with sliding time.

When the concentration of $TiO_2/Ti_3C_2T_x$ hybrid nanocomposites is 1 wt%, the best antifriction performance is achieved. The remarkable tribological property may due to their TiO_2 nanoparticles and thin laminated structure. Furthermore,
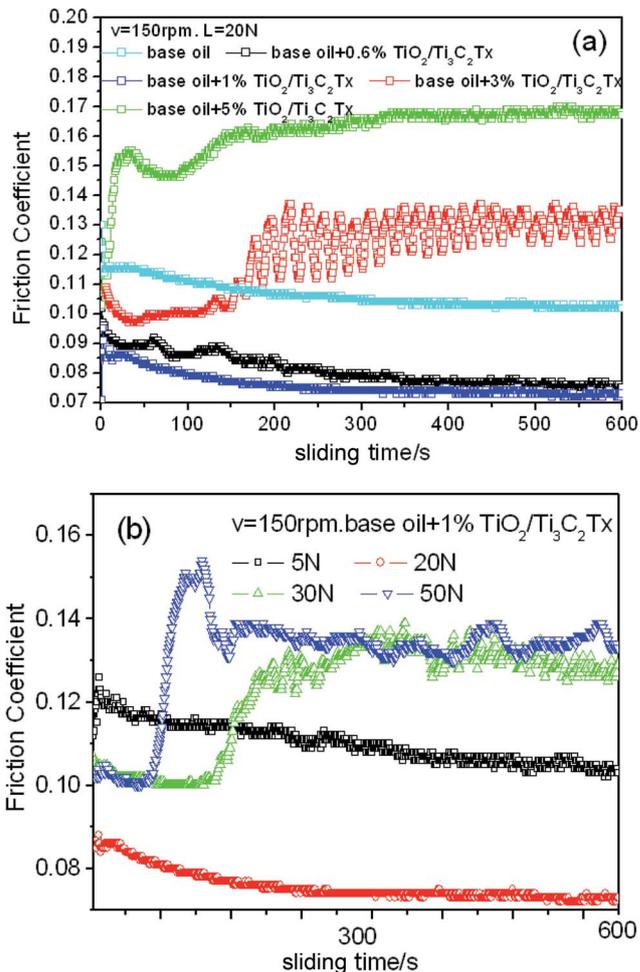
the nanoparticles can readily enter into the boundary with base oil and form a uniform shielded film, so the behavior of friction coefficient is more steady than others, but too much higher concentration of the nanoparticles revealed vast agglomeration, could not enter the contact area easily,[38,39] also could damage the consistency of the gluey system of the base oil.[40] So, the optimum concentration of the $TiO_2/Ti_3C_2T_x$ hybrid nanocomposites as an additive in base oil is proposed to be 1 wt%.

Fig. 5b reveals the change of friction coefficient of 1 wt% $TiO_2/Ti_3C_2T_x$ hybrid nanocomposites as an additive of lubricant under different loads, respectively. It can be observed that there is a trend that the friction coefficient of nanocomposites decreases firstly and then increases as the load increases, also, the curves of 30 N and 50 N have higher undulation than the curves of 5 N and 20 N. We can get the ideal load for friction display at 20 N. Within the scope of certain pressure, $TiO_2/Ti_3C_2T_x$ hybrid nanocomposites is delaminated readily at the contact region and precipitate a tribofilm, which can reduce shearing stress and generate a low friction coefficient. When the applied load is 5 N, $TiO_2/Ti_3C_2T_x$ cannot be compacted on the
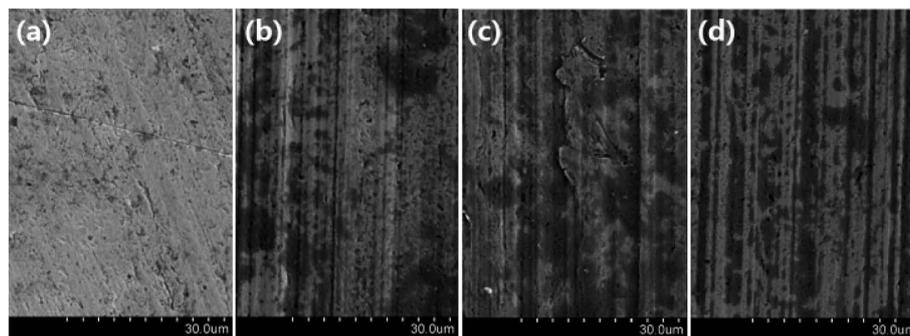
Fig. 6 SEM images of the grinding cracks lubricated by base oil with different concentrations 0 wt% (a), 0.6 wt% (b), 3.0 wt% (c), and 5.0 wt% (d) hybrid nanocomposites.

friction surface to repair grinding crack, so the protective film was not shaped. Otherwise, if the applied load is too high, the protective film at the region will be damaged, finally inducing high undulation and friction coefficient.

With the aim of study the wear resistance performance of $TiO_2/Ti_3C_2T_x$ hybrid nanocomposites as lubricant oil additives, the grinding cracks of plate after friction were examined by SEM and BRUKER ContourGT non-contact 3D optical profile testing apparatus.

SEM photographs of the worn scar lubricated by base oil with different concentrations of $TiO_2/Ti_3C_2T_x$ hybrid nano-composites under 20 N are given in Fig. 6 and 7a. Fig. 6a presents that the rubbed surface lubricated by the pure base oil is quite rough with lots of wide and deep furrows along the sliding direction because of contact fatigue. In Fig. 6b and 7a, the worn surface lubricated with base oil added 0.6 and 1.0 wt% $TiO_2/Ti_3C_2T_x$ hybrid nanocomposites is smoother than that lubricated with pure base oil. The furrows are shallower and subtler on the worn surface of steel disc under the lubrication of base oil with 0.6 and 1.0 wt% $TiO_2/Ti_3C_2T_x$, meanwhile, a thin tribofilm is formed on the substrate. However, the wear scar becomes obviously rough and the plastic deformation is severe when 3.0 wt% and 5.0 wt% $TiO_2/Ti_3C_2T_x$ were added into the base oil, which is well corresponded to the unstable and higher friction coefficient, as shown in Fig. 5a. It can be inferred that the tribological properties of the base oil could be significantly improved by adding the $TiO_2/Ti_3C_2T_x$ hybrid nanocomposites as

additives, though the content of $TiO_2/Ti_3C_2T_x$ must be controlled at a reasonable level. Too much $TiO_2/Ti_3C_2T_x$ may act as superfluous abrasive particles and result in the deterioration of the friction conditions.

The morphology of the grinding crack lubricated by base oil with 1 wt% $TiO_2/Ti_3C_2T_x$ hybrid nanocomposites under 20 N and 50 N was observed using SEM, as revealed in Fig. 7. This SEM image in Fig. 7a shows that the friction surface lubricated by the base oil with 1 wt% $TiO_2/Ti_3C_2T_x$ hybrid nanocomposites under 20 N is glossy. The furrows are shallow and no distinct mechanical damage on the worn surface of steel disc, meanwhile, a light tribofilm is shaped on the substrate. However, under the load 50 N, as shown in Fig. 7b, the worn surface proves clearly coarse and the plastic deformation is rigorous, which is consistent with the higher and labile friction coefficient, as shown in Fig. 5b.

Fig. 8 illustrates grinding crack of the base oil with 1 wt% $TiO_2/Ti_3C_2T_x$ hybrid nanocomposites at 150 rpm for 600 s under the load of 20 N and 50 N. It can be distinct observed that the grinding crack under 20 N is composed of glossy and shallow furrows along the sliding direction (Fig. 8a), and the grinding crack caused by under 50 N (Fig. 8b) is wider and distributed irregular pits. From the images we can see that the depth and width of the wear scar for 20 N are about 30 μm and 280 μm respectively, while those for 50 N are about 35 μm and 400 μm. This manifests that the base oil with $TiO_2/Ti_3C_2T_x$ hybrid nanocomposites under 20 N shown better anti-wear ability than 50 N.

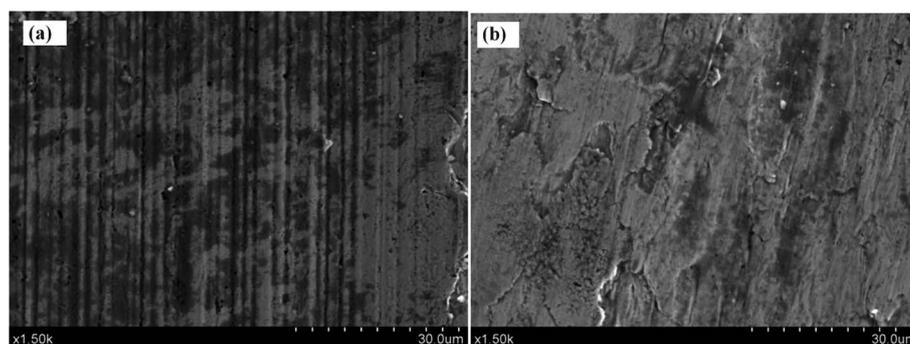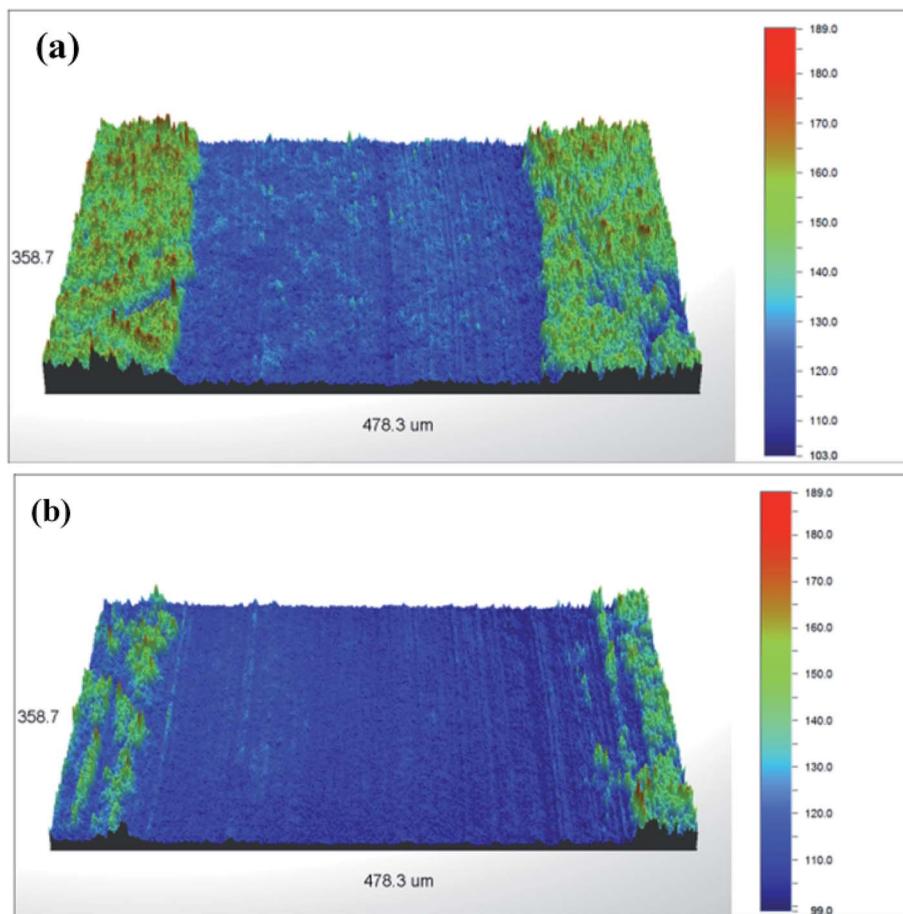**Fig. 7** SEM images of the grinding crack lubricated by base oil with 1.0 wt% $TiO_2/Ti_3C_2T_x$ hybrid nanocomposites under (a) 20 N and (b) 50 N.

Fig. 8 Non-contact 3D optical profile testing instrument images of the grinding crack of the base oil with 1 wt% $TiO_2/Ti_3C_2T_x$ hybrid nano-composites under (a) 20 N and (b) 50 N.
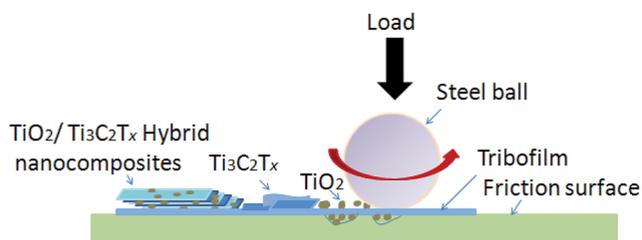

Fig. 9 Tribological mechanism model of the base oil with $TiO_2/Ti_3C_2T_x$ hybrid nanocomposites.

The tribological tests and morphology of the grinding crack results suggest that the 1 wt% $TiO_2/Ti_3C_2T_x$ nanocomposites with the optimal load (*e.g.*, 20 N) aids to form continuous and uniform tribofilm on the rubbing surface leading to friction reduction.

The tribological mechanism between the rubbing surfaces in base oil with $TiO_2/Ti_3C_2T_x$ hybrid nanocomposites is iconically presented in Fig. 9. It is believed that the suitable content of $TiO_2/Ti_3C_2T_x$ hybrid nanocomposites under appropriate load could enter in the gap between the friction surfaces easily. During sliding, the desquamated TiO_2 particles can mending

the scratched surface to decrease the contact of rough between the friction surfaces, meanwhile the exfoliated $Ti_3C_2T_x$ sheets adsorb onto the rubbing surface and form a tribofilm, which can decrease shearing stress and the direct contact of tribopair, this is the main mechanism for improving the tribological behavior of $TiO_2/Ti_3C_2T_x$ hybrid nanocomposites.

4.   Conclusion

In brief, $TiO_2/Ti_3C_2T_x$ hybrid nanocomposites were prepared by a liquid-phase reaction route. At a lower concentration (1 wt%) with the optimal load (*e.g.*, 20 N), $TiO_2/Ti_3C_2T_x$ hybrid nano-composites could effectively improve the tribological properties of base oil by synergistic effects of mending the scratched surface and formation of a uniform tribofilm on the surface, which prevent the direct contact between counterparts during the friction process. This study suggests $TiO_2/Ti_3C_2T_x$ hybrid nanocomposites exhibit a potential application as oil-based lubricant additives.

Acknowledgements

Notes and references

1 G. W. Bentzel, M. Ghidiu and J. Griggs, On the Interactions of Ti_2AlC, Ti_3AlC_2, Ti_3SiC_2 and Cr_2AlC with Pure Sodium at 550 °C and 750 °C, *Corros. Sci.*, 2016, **111**, 568–573.

2 S. Gupta, T. Hammann and R. Johnson, Tribological behavior of novel Ti_3SiC_2 (natural nanolaminates)-reinforced epoxy composites during dry sliding, *Tribol. Trans.*, 2015, **58**, 560–566.

3 M. Xue, H. Tang and C. S. Li, Preparation and tribological behaviour of laminated Ti_3AlC_2 crystals as additive in base oil, *Adv. Appl. Ceram.*, 2014, **113**, 245–250.

4 A. Mockuté, J. Lu and E. J. Moon, Solid solubility and magnetism upon Mn incorporation in the bulk ternary carbides Cr_2AlC and Cr_2GaC, *Mater. Res. Lett.*, 2015, **3**, 16–22.

5 I. R. Shein and A. L. Ivanovskii, Graphene-like nanocarbides and nanonitrides of d metals (MXenes): synthesis, properties and simulation, *Micro Nano Lett.*, 2013, **8**, 59–62.

6 M. Xue, X. Zhang, H. Tang and C. S. Li, Synthesis of high purity Cr_2AlC nanolamellas with improved tribological properties for oil-based additives, *RSC Adv.*, 2014, **4**, 39280–39286.

7 M. Beckers, N. Schell and R. M. S. Martins, Phase stability of epitaxially grown Ti_2AlN thin films, *Appl. Phys. Lett.*, 2006, **89**, 74101–74103.

8 Z. Huang, H. Zhai and W. Zhou, Tribological behaviors and mechanisms of Ti_3AlC_2, *Tribol. Lett.*, 2007, **27**, 129–135.

9 M. W. Barsoum, H. I. Yoo and I. K. Polushina, Electrical conductivity, thermopower, and hall effect of Ti_3AlC_2, Ti_4AlN_3, and Ti_3SiC_2, *Phys. Rev. B: Condens. Matter Mater. Phys.*, 2000, **62**, 1055051–1110198.

10 X. H. Wang and Y. C. Zhou, Layered machinable and electrically conductive Ti_2AlC and Ti_3AlC_2 ceramics: a review, *J. Mater. Sci. Technol.*, 2010, **26**, 385–416.

11 Y. W. Bao and Y. C. Zhou, Evaluating high-temperature modulus and elastic recovery of Ti_3SiC_2 and Ti_3AlC_2 ceramics, *Mater. Lett.*, 2003, **57**, 4018–4022.

12 X. H. Wang and Y. C. Zhou, Oxidation behavior of Ti_3AlC_2 at 1000–1400 °C in air, *Corros. Sci.*, 2003, **45**, 891–907.

13 J. X. Chen, Y. C. Zhou and H. B. Zhang, Thermal stability of Ti_3AlC_2/Al_2O_3 composites in high vacuum, *Mater. Chem. Phys.*, 2007, **104**, 109–112.

14 N. V. Tzenov and M. W. Barsoum, Synthesis and Characterization of Ti_3AlC_2, *J. Am. Ceram. Soc.*, 2000, **83**, 825–832.

15 M. W. Barsoum, Physical Properties of the MAX Phases, *Encyclopedia of Materials Science & Technology*, 2006, vol. 160, pp. 1–11.

16 F. Chang, C. Li, J. Yang, M. Xue, H. Tang and C. S. Li, Synthesis of a new graphene-like transition metal carbide by de-intercalating Ti_3AlC_2, *Mater. Lett.*, 2013, **109**, 295–298.

17 M. Naguib, M. Kurtoglu and V. Presser, Two-Dimensional Nanocrystals Produced by Exfoliation of Ti_3AlC_2, *Adv. Mater.*, 2011, **23**, 4248–4253.

18 M. Naguib, O. Mashtalir and J. Carle, Two-dimensional transition metal carbides, *ACS Nano*, 2012, **6**, 1322–1331.

19 M. Ghidiu, M. Naguib and C. Shi, Synthesis and characterization of two-dimensional Nb_4C_3 (MXene), *Chem. Commun.*, 2014, **50**, 9517–9520.

20 V. Presser, M. Naguib and L. Chaput, Erratum: First-order Raman scattering of the MAX phases: Ti_2AlN, $Ti_2AlC_{0.5}N_{0.5}$, Ti_2AlC, $(Ti_{0.5}V_{0.5})_2AlC$, V_2AlC, Ti_3AlC_2, and Ti_3GeC_2, *J. Raman Spectrosc.*, 2013, **44**, 1060.

21 M. Naguib, V. N. Mochalin and M. W. Barsoum, 25th Anniversary Article: MXenes: A New Family of Two-Dimensional Materials, *Adv. Mater.*, 2014, **26**, 992–1005.

22 M. Khazaei, M. Arai and T. Sasaki, Novel Electronic and Magnetic Properties of Two-Dimensional Transition Metal Carbides and Nitrides, *Adv. Funct. Mater.*, 2013, **23**, 2185–2192.

23 J. Halim, K. M. Cook and M. Naguib, X-ray photoelectron spectroscopy of select multi-layered transition metal carbides (MXenes), *Appl. Surf. Sci.*, 2015, **362**, 406–417.

24 Y. Bai, K. Zhou and N. Srikanth, Dependence of elastic and optical properties on surface terminated groups in two-dimensional MXene monolayers: a first-principles study, *RSC Adv.*, 2016, **6**, 35731–35739.

25 B. Anasori, Y. Xie and M. Beidaghi, Two-dimensional, ordered, double transition metals carbides (MXenes), *ACS Nano*, 2015, **9**, 9507–9516.

26 Q. Tang, Z. Zhou and P. Shen, Are MXenes promising anode materials for Li ion batteries? Computational studies on electronic properties and Li storage capability of Ti_3C_2 and $Ti_3C_2X_2$ (X = F, OH) monolayer, *J. Am. Chem. Soc.*, 2012, **134**, 16909–16916.

27 Z. Guo, L. Zhu and J. Zhou, Microscopic origin of MXenes derived from layered MAX phases, *RSC Adv.*, 2015, **5**, 25403–25408.

28 Y. Liu, X. Zhang and S. Dong, Synthesis and tribological property of $Ti_3C_2T_x$ nanosheets, *J. Mater. Sci.*, 2016, 1–10.

29 D. Sun, M. Wang and Z. Li, Two-dimensional Ti_3C_2, as anode material for Li-ion batteries, *Electrochem. Commun.*, 2014, **47**, 80–83.

30 S. Hosseini, H. Jahangirian and T. J. Webster, Synthesis, characterization, and performance evaluation of multilayered photoanodes by introducing mesoporous carbon and TiO_2 for humic acid adsorption, *Int. J. Nanomed.*, 2016, **11**, 3969–3978.

31 Z. Hong, K. Zhou and J. Zhang, Self-Assembled Synthesis of Mesocrystalline TiO_2@C-rGO Hybrid Nanostructures for Highly Reversible Sodium Storage, *Cryst. Growth Des.*, 2016, 6605–6612.

32 M. Wongaree, S. Chiarakorn and S. Chuangchote, Photocatalytic performance of electrospun CNT/TiO_2 nanofibers in a simulated air purifier under visible light irradiation, *Environ. Sci. Pollut. Res.*, 2016, 1–12.

33 L. Qian, S. Yang and W. Hong, Synthesis of Biomorphic Charcoal/TiO$_2$ Composites from Moso Bamboo Templates for Absorbing Microwave, *BioResources*, 2016, **11**, 7078–7090.

34 M. Naguib, O. Mashtalir and M. R. Lukatskaya, One-step synthesis of nanocrystalline transition metal oxides on thin sheets of disordered graphitic carbon by oxidation of MXenes, *Chem. Commun.*, 2014, **50**, 7420–7423.

35 Y. Gao, H. Chen and A. Zhou, Novel Hierarchical TiO$_2$/C Nanocomposite with Enhanced Photocatalytic Performance, *Nano Brief Reports & Reviews*, 2015, **10**, 1550064–1550065.

36 J. Come, J. M. Black and M. R. Lukatskaya, Controlling the actuation properties of MXene paper electrodes upon cation intercalation, *Nano Energy*, 2015, **17**, 27–35.

37 S. J. Kim, M. Naguib and M. Zhao, High mass loading, binder-free MXene anodes for high areal capacity Li-ion batteries, *Electrochim. Acta*, 2015, **163**, 246–251.

38 G. Tang, J. Zhang and C. Liu, Synthesis and tribological properties of flower-like MoS$_2$, microspheres, *Ceram. Int.*, 2014, **40**, 11575–11580.

39 M. Zhang, B. Chen and H. Tang, Hydrothermal synthesis and tribological properties of FeS$_2$ (pyrite)/reduced graphene oxide heterojunction, *RSC Adv.*, 2014, **5**, 1417–1423.

40 G. Zhao, Q. Zhao, W. Li, X. Wang and W. Liu, Tribological properties of nano-calcium borate as lithium grease additive, *Lubr. Sci.*, 2014, **26**, 43–53.